Kapal: Jurnal Ilmu Pengetahuan dan Teknologi Kelautan
(Kapal: Journal of Marine Science and Technology)
journal homepage: http://ejournal.undip.ac.id/index.php/kapal
2301-9069 (e)
1829-8370 (p)

CFD Analysis of Interference Factor in Hydrofoil-Supported Catamarans (HYSUCAT)

Ahmad Firdhaus[1) *)], Kiryanto[1)], Good Rindo[1)], Andi Trimulyono[1)]

[1)] Department of Naval Architecture, Faculty of Engineering, Universitas Diponegoro, Semarang, Indonesia
[*)] Corresponding Author: ahmadf@lecturer.undip.ac.id

Article Info

Keywords:
Hydrofoil Supported;
Catamaran;
Ship Resistance;
Interference Factor;
CFD;

Article history:
Received: 24/01/2024
Last revised: 26/02/2024
Accepted: 28/02/2024
Available online: 29/02/2024
Published: 29/02/2024

DOI:
https://doi.org/10.14710/kapal.v21i1.61750

Abstract

Catamaran, with its distinctive dual-hull design, offers unique advantages in maritime applications, including improved stability and space utilization over traditional monohull vessels. However, the interaction between the two hulls generates complex hydrodynamic phenomena, significantly influencing the vessel's overall performance. One critical aspect of this interaction is the interference factor, which affects the hydrodynamic resistance encountered by the vessel. The purpose of this paper is to investigate the changes in hydrodynamic characteristics that occur when hydrofoils are incorporated into typical catamaran hull forms. This is accomplished through the utilization of advanced Computing Fluid Dynamics (CFD) simulations. In this study, a Delft-372 catamaran with a concept design is modified by installing a foil system with a high Reynolds number in order to reduce its overall resistance. The new system is then analyzed in order to determine the impact that it has on interference factors. For the purpose of achieving a comprehensive understanding of hydrodynamic behavior, the simulations are carried out under a variety of operating conditions, which include a variety of speeds. Simulations result indicate that the interference factor consistently increases drag for hydrofoil-supported catamarans to more than double that of monohulls across all speeds, particularly when hydrofoil-induced flow disturbances adversely affect the hull's boundary layer, leading to reduced efficiency.

1. Introduction

The exploration of hydrodynamic efficiency in marine vessels has been a pivotal aspect of naval engineering, leading to the advent of innovative designs and technologies. In this context, the hydrofoil-supported catamaran, a vessel type that combines the stability and space of catamarans with the speed and efficiency of hydrofoils, represents a significant evolution in naval architecture [1], [2]. The incorporation of hydrofoils in catamarans introduces a new dimension to the study of hydrodynamic interference factors, which are crucial in determining the performance and operational efficiency of these vessels.

Hydrofoils, structured as submerged wings, are designed to lift a vessel's hull above the water surface at higher speeds, reducing drag and enhancing efficiency [3], [4], [5]. The use of hydrofoils in catamaran design has been a subject of ongoing research and development. Hoppe [6], [7] discuss the application of hydrofoil-supported catamarans, with the former highlighting the performance of various models and the latter focusing on the optimization of these designs. Calkins [8] introduces the concept of a hybrid hydrofoil catamaran, which combines static and dynamic support for improved stability and performance. Miyata [9] presents a specific design for a new-type hydrofoil catamaran, emphasizing its smooth transition between hull-borne and foil-borne conditions. Collectively, these studies underscore the potential of hydrofoil-supported catamarans to achieve enhanced speed, stability, and efficiency.

The interference factors in catamarans are influenced by a multitude of variables, including hull separation, hydrofoil configuration, vessel speed, and environmental conditions [10], [11]. These factors include increased wave-making resistance, uneven pressure distribution, flow separation, vortex shedding, and altered seakeeping behavior, collectively impacting the vessel's performance, stability, and efficiency. Designing and optimizing catamarans requires addressing these interference factors, often through numerical simulations and hydrodynamic analyses, to ensure their suitability for diverse marine applications.

A series of numerical studies have explored the impact of various factors on the hydrodynamic performance of hydrofoil-supported catamarans. Research on catamaran interference factors has shown that the distance between the hulls and the vessel's speed significantly impacts these factors [12]. The interaction effects on a catamaran traveling with forward speed in waves have been found to be complex, making seakeeping prediction challenging [13]. Zhou [14] and Wang

[15] both found that the installation of a stern flap can reduce resistance and improve sailing attitude, particularly at high speeds and in regular head waves. Kumari [16] further investigated the effects of different hydrofoil configurations on lift and drag coefficients, with a tandem arrangement showing higher lift coefficients. Castiglione [17] focused on the interference effects of wave systems on a multi-hull vessel in shallow water, finding that water depth and separation distance significantly influence resistance and interference. Collectively, these studies highlight the potential for hydrofoils to enhance the performance of hydrofoil-supported catamarans, particularly in reducing resistance and improving sailing attitude [18].

This work advances hydrodynamic studies in maritime vessels, particularly hydrofoil-supported catamarans. Hydrofoils' benefits in monohull designs are well-documented, but their effects on catamarans' dual-hull layout, especially in a hydrofoil-supported setup, are not. This research gap highlights the need to study how hydrofoils alter catamaran hull interference parameters such as ship resistance, wave distribution, and interference factor. The Delft-372 catamaran model will be utilized in this investigation since it has extensive experiments and numerical simulations currently accessible in the literature [10], [11], [19], [20], [21]. This will make it easy to check and validate calculations derived from the simulation results. A 4-digit NACA 4412 airfoil with a high Reynolds number will be mounted on the hull of the Delft-372 catamaran. The project examines hydrofoils and catamaran hulls to produce more efficient, stable, and high-performing marine boats. This study should help naval architects, marine engineers, and the maritime sector build and optimize future ship design.

2. Methods

2.1. Modeling, meshing, and boundary conditions

The Delft-372 Catamaran Hull [22], as shown in Table 1, represents a high-speed catamaran hull that was investigated in the present study. The catamaran's hydrofoil system employs a NACA 4412 airfoil designed for a High Reynolds number. The airfoil has explicitly been positioned on the hull of the Delft-372 catamaran.[23], [24]

Table 1. Principal dimension of the Delft-372 Catamaran Hull [22]

Dimension	Symbol	Value
Length between perpendiculars (m)	L_{pp}	3.00
Beam overall (m)	B	0.94
Beam demi hull (m)	b	0.24
Distance between center of hulls (m)	H	0.7
Draught (m)	T	0.15
Displacement (kg)	Δ	87.07
Vertical centre of gravity (m)	V_{CG}	0.34
Longitudinal center of gravity (m)	L_{CG}	1.41

The Delft-372 catamaran's NACA 4412 foil system is seen in Figure 1. The hydrofoil system has two foils, one in front and one behind the vessel. Figure 1b depicts foil longitudinal placement, whereas Figure 1c displays submerged depth. Submerged depth of foils was computed using h/c = 0.4, where h is submerged depth and c is hydrofoil chord length [25]. The foils' span equals the catamaran's 0.7-meter hull difference. Foils have a 10-centimetre chord length, or 0.10 meters. Foil aspect ratio (AR) is 7, which is the span (s) to chord (c) ratio. A previous study on the NACA 4412 found that the greatest lift-to-drag ratio is between 4° and 6° [26], [27]. Foils were set at a 5.25° angle of attack, measured counterclockwise from the vessel's course direction, the positive x-axis.

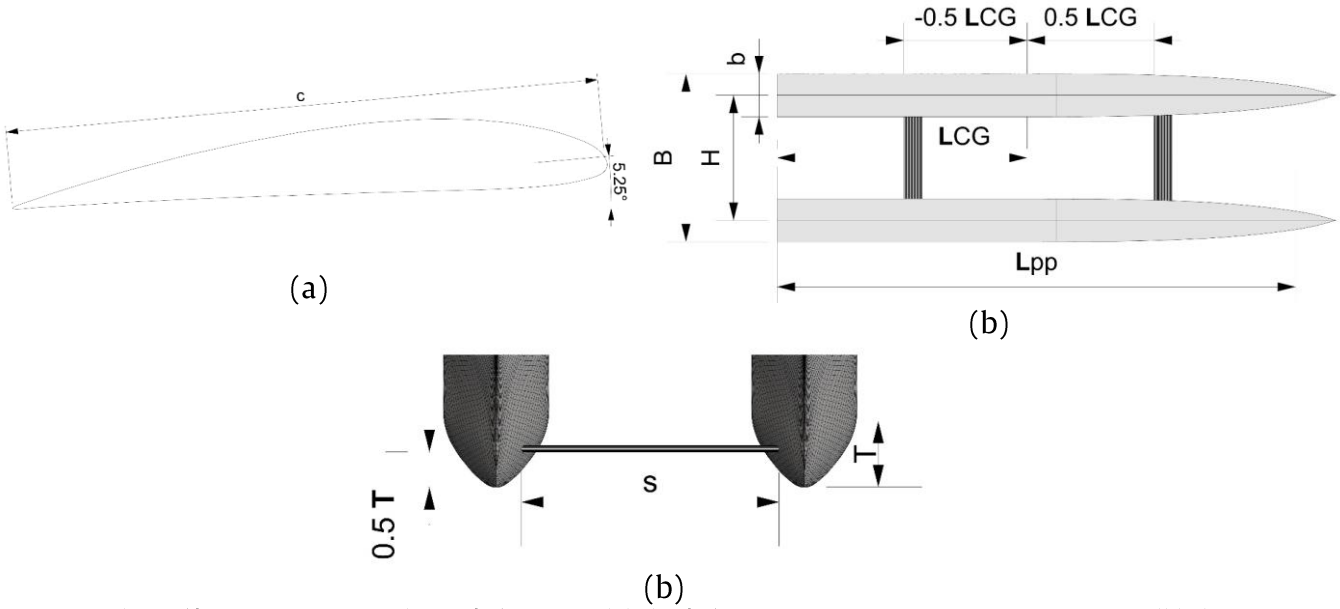

Figure 1. The Delft-372 catamaran's hydrofoil system: (a) the foil arrangement according to NACA 4412, (b) the position of the foils in relation to depth, and (c) the location of the hydrofoils throughout the boat's length.

Figure 2 depicts the computational domain together with boundary conditions drawn from existing literature [28]. The intake was located 1L upstream of the model. The outlet was located 3L aft, in close proximity to the model's rear. The distance between the sidewall and the waterline was 1.5 times the length (L). The inlet, exit, and sidewall boundary conditions were characterized by an identical free stream far-field velocity. Establish the boundary conditions by choosing a constant pressure and positioning the lower and upper walls at distances of 1.5 and 1 times the length of the model below and above it, respectively. The boundary condition for the ship's hull was set as a wall function to prevent any sliding. The simulations accurately determined the vertical and rotational motions of the object.

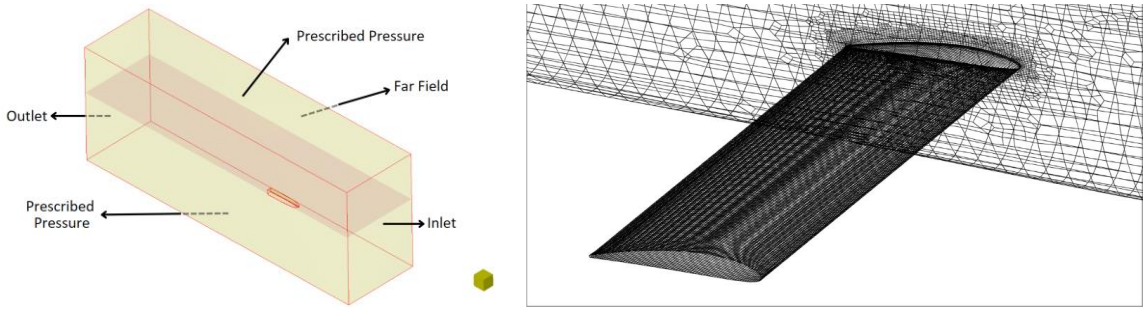

Figure 2. Computational domain and boundary conditions with the simulation model (a) and detail mesh on the surface of the simulation model (b)

2.2. Free-surface solver

Potential flow analysis in modern fluid dynamics simulations often employs boundary element methods to explore free surface wave generation. Specifically, the Rankine source method within potential flow frameworks is pivotal for studying the interactions between ship hulls and waves, crucial for simulating wave resistance. When addressing complexities related to free surface phenomena such as wave-making resistance, viscous flow simulations are essential. These simulations typically adopt two primary methodologies for free surface computations: the interface-tracking approach, often realized through dynamic mesh adjustments, and the interface-capturing technique, commonly referred to as the Volume of Fluid (VoF) method [29], [30].

In simulating a ship's performance in planning, numerical models take into account different speeds, angles of attack, and trim angles. These problems with fluid flow are handled by the ISIS-CFD solver, which uses the incompressible unsteady Reynolds-averaged Navier Stokes equations. The spatial discretization of transport equations is accomplished using a finite volume approach. Unstructured meshes, whether two-dimensional, three-dimensional, or rotationally symmetric, may be discretized using a face-based approach. Meshes like this create control volumes that don't overlap and are bounded by different characteristics. In isothermal circumstances, the flow of incompressible multi-phase viscous fluids is controlled by the mass, momentum, and volume fraction conservation equations, as shown in Equations (1-3).

$$\frac{\partial}{\partial t}\int_v \rho\, dV + \int_S \rho(\mathbf{U}-\mathbf{U}_d).\mathbf{n}\, dS = 0 \tag{1}$$

$$\frac{\partial}{\partial t}\int_v \rho\, U_i dV + \int_S \rho U_i(\mathbf{U}-\mathbf{U_d}).\boldsymbol{n}\, dS = \int_S (\tau_{ij} I_j - pI_i).\mathbf{n}\, dS + \int_S \rho g_i\, dV \tag{2}$$

$$\frac{\partial}{\partial t}\int_v c_i\, dV + \int_S c_i(\mathbf{U}-\mathbf{U}_d).\mathbf{n}\, dS = 0 \tag{3}$$

The control volume V is defined by a closed surface S, moving at a velocity. $\mathbf{U}_d$ And enclosed by an outward-pointing unit normal vector $\mathbf{n}$. The velocity ($\mathbf{U}$) and pressure (ρ) fields are considered, where I_j It is a vector with the j component as 1. I_j represents the viscous stress tensor and g_i It is the gravity vector. The volume fraction c_i Indicates the presence or absence of fluid i.

$$\frac{\partial}{\partial t}(\rho k) + \frac{\partial}{\partial x_i}(\rho k u_i) = \frac{\partial}{\partial x_j}\left(\Gamma_k \frac{\partial_k}{\partial x_j}\right) + G_k - Y_k \tag{4}$$

$$\frac{\partial}{\partial t}(\rho \omega) + \frac{\partial}{\partial x_i}(\rho \omega u_i) = \frac{\partial}{\partial x_j}\left(\Gamma_\omega \frac{\partial_\omega}{\partial x_j}\right) + G_\omega - Y_\omega + D_\omega \tag{5}$$

The SST (shear-stress transfer) model, developed by F.R. Menter [31], [32], stems from two-equation models and offers several benefits. It combines coefficients zonally and limits eddy viscosity growth in rapidly strained flows. The model employs Wilcox's model near solid walls and the standard model at the edges of boundary layers and free-shear layers. Shear stress transport modeling, by restricting turbulent shear stress to a constant multiple of turbulent kinetic energy within boundary layers, improves predictions in flows with strong pressure gradients and separation [33]. The SST k-ω model's transport equations are outlined in Equations (4-5), addressing the generation of turbulent kinetic energy (G_k), its dissipation (Y_k), and the generation of ω (G_ω), along with its dissipation (Y_ω) and cross-diffusion term (D_ω). The effective diffusivities of

k and ω are denoted as Γ_k and Γ_ω, respectively. This turbulence model enables accurate predictions of flow separation onset and intensity.

2.3. Grid independency

Evaluating solution stability in relation to mesh density is crucial. A solution achieves mesh independence when additional mesh refinement no longer significantly impacts the results. Ensuring that solutions are both stable and mesh-independent is vital for the credibility of the outcomes. Systematic grid independence tests were conducted to identify the ideal mesh size (total cell count) and verify the convergence of the numerical solution against the criterion of grid independence. These tests involved calculating the total ship resistance (RT) while progressively increasing the mesh density. Simulations were executed, with each iteration expanding the grid count by a factor of 1.5 to 2. The duration of each simulation was recorded and compared with others, expressing the variance in percentages.

Figure 3 shows the relationship between ship resistance and the number of simulation cells and shows a trend toward convergence. The cell count trends towards an asymptotic value as it increases indefinitely. The determined optimal cell count stands at approximately 1.91 x 10^6 cells (observed in the 5th run), presenting a negligible error margin of 0.63%, well below the 2% threshold commonly cited in the relevant literature.

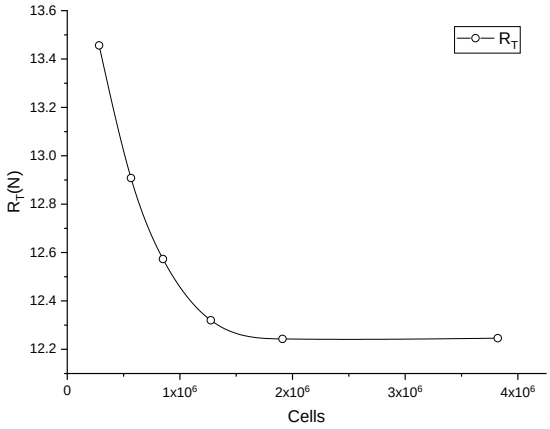

Figure 3. Overall vessel drag function (R_T) represents the total number of cells used in the simulation.

3. Results and Discussion

This chapter of the research article presents the pivotal findings derived from the Computational Fluid Dynamics (CFD) simulations, mainly focusing on the total drag coefficient in hydrofoil-supported catamaran ships. Our study embarked on an explorative journey to unravel the dynamics of hydrofoils and their influence on the drag and resistance properties of catamarans at varying speeds. The Computational Fluid Dynamics (CFD) simulations conducted in this study primarily focused on evaluating the total ship resistance under various operational scenarios. The results depicted a comprehensive picture of how different factors, such as vessel speed, hull geometry, and environmental conditions, influence the total resistance encountered by the ship.

As shown in Figure 4, numerical simulations revealed a consistent increase in total resistance with the augmentation of vessel speed. This trend aligns with theoretical predictions, indicating that the square of the speed significantly impacts resistance. Notably, at higher speeds, a marked increase in wave-making resistance was observed, contributing substantially to the total resistance. The resistance value on a hydrofoil-supported catamaran (hysucat) ship is smaller than that of a regular catamaran at a certain speed, notably Fr = 1-1.4 with a drag reduction up to % because the hydrofoil design allows the ship to "lift" part of its body above the water surface. This means that at a given speed, the bottom of the hysucat vessel has less contact with the water, which reduces frictional resistance and wave resistance compared to a regular catamaran where the entire body is in contact with the water.

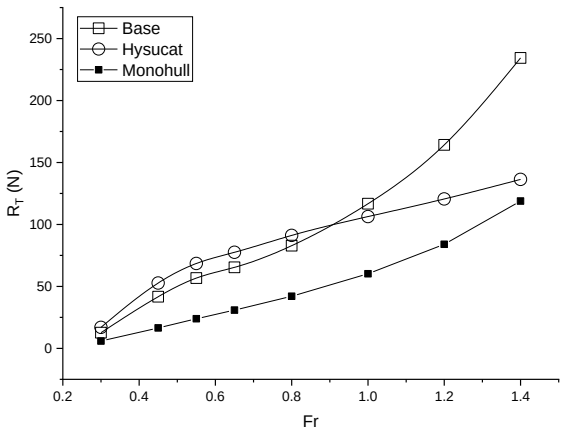

Figure. 4. Total ship resistance value (R_T) as a function of ship speed (Fr)

Figure 5 demonstrates that implementing a hydrofoil system for retrofitting purposes leads to a decrease in the overall wetted surface area (WSA) of the vessel. As the vessel accelerates, it produces extra upward force, which helps to hold up both sections of the hull partially. This alteration in WSA is analogous to the scenario in which the hydrofoils are disengaged while the primary hydrofoil remains wholly submerged. At increased velocities, the hull experiences a significant upward force, resulting in a decrease in wetted surface area (WSA) of up to 49% caused by the vessel's inclination, enabling the hydrofoil to penetrate the water's surface. Within this context of high velocity, the resistance is prone to augment as the pitch angle rises, principally because the main hydrofoil experiences a substantial decrease in lift. As the pitch angle of a catamaran increases, its water surface area (WSA) decreases until the hull is visible above the water line, which is anticipated to reduce the vessel's resistance. The use of hydrofoils offers a heightened level of complexity as the lift diminishes as a result of the vessel's pitch angle, thus leading to an augmentation in the wing's surface area.

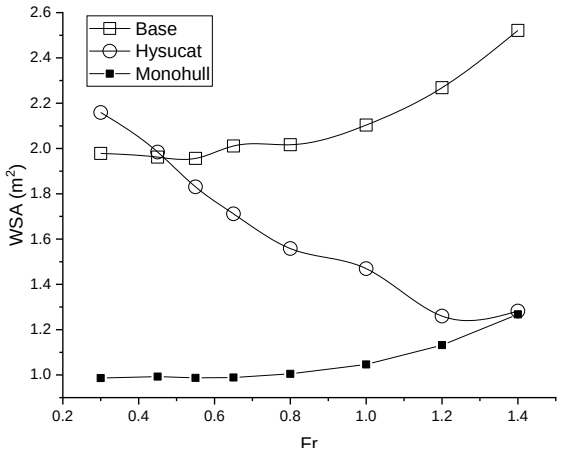

Figure 5. Wetted surface area (m^2) as a function of ship speed (Fr)

The observed increased drag coefficient of approximately 14-42% across all speeds can be attributed to the additional surface area and the induced drag presented by the hydrofoils, as shown in Figure 6. However, the reduction in total resistance at certain speeds likely results from the lift generated by the hydrofoils, which offsets a portion of the hull's weight from the water. This lift effect, especially prominent at specific speed ranges, reduces the wetted surface area of the hulls, thereby decreasing the overall resistance. These findings have profound implications for the design and operational strategies of hydrofoil-supported catamarans. The increased drag coefficient suggests a need for careful consideration of hydrofoil design to optimize performance. Meanwhile, the reduced total resistance at certain speeds highlights the potential for enhanced efficiency in hydrofoil-supported catamarans under specific operating conditions.

In the context of drag on hydrofoil-supported catamaran (hysucat) ships, several factors cause the total drag coefficient to be generally more significant at all speeds. First, although hydrofoils are effective at reducing friction and wave resistance, their design aimed at generating lift inherently creates additional drag. This process of lifting part of the ship above the water requires significant energy. Second, the complexity of hysucat designs, which often include features such as wings and additional components, increases aerodynamic and hydrodynamic drag. Third, at low speeds, before the hydrofoil operates efficiently, the hysucat can experience higher resistance compared to an ordinary catamaran. Fourth, at high speeds, the drag caused by the hydrofoil, especially the induced drag, becomes very influential. Although at certain speeds, the HSC can be more efficient due to lower frictional resistance with the water, overall, this hydrofoil design adds complexity and drag, thereby increasing the total drag coefficient at all speeds.

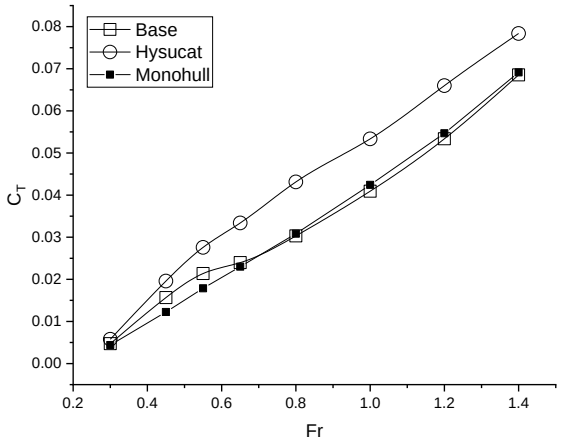

Figure 6. Total Resistance coefficient (C_T) versus ship speed (Fr)

The interference effects between the hydrofoils and the hulls were also analyzed in Figure 7. By taking into account the interference factor IF –the relative difference between the resistance coefficients of the catamaran and the monohull–we may better understand the impact that changes in hull separation have on the overall resistance [34]. This is defined by

$$\mathrm{IF} = \frac{C_T^{(C)} - C_T^{(M)}}{C_T^{(M)}} \tag{6}$$

The superscripts M and C in this phrase denote the monohull and catamaran, respectively. Figure 7 shows, parametrically, the relationship between hull separation and the interference factor's fluctuation with the Froude number. It is evident from the graph that the interference factor is often positive, meaning that the catamaran will typically encounter drag that is more than double that of the monohull. The simulations showed that at all ship speeds, the interference could lead to increased drag and reduced efficiency. This was particularly evident in scenarios where the hydrofoil-induced flow disturbances interacted adversely with the hull's boundary layer. In such configurations, the flow from the hydrofoils directly impacted the hulls, leading to increased drag and a notable reduction in overall hydrodynamic efficiency. This effect was particularly evident in the case of catamarans with shorter hull separations, where the proximity of the hydrofoils to the hulls was unavoidable. However, with careful design optimization, these adverse effects can be minimized.

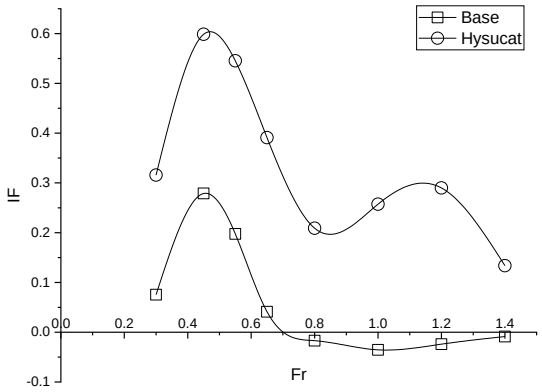

Figure 7. Interference Factor (IF) as a function of ship speed (Fr)

Figure 8 shows the wave-fields produced by the catamaran models at various Froude numbers as contour lines of the nondimensional free-surface elevation, which are Fr 0.55. Different values of the catamaran model are represented by the panels in each figure. Each ta also includes the wave field surrounding the monohull for reference. While free-surface disturbances are often found to be amplified on the outside of the vessel, variations between the monohull, catamaran, and hysucat are still discernible at this Fr value of 0.55. One example is the greatly amplified bow wave, which causes a large portion of the ship's model to depressurize. Within the inner area, the wave field is defined by a long and narrow peak that arises from the merging of the two bow crests.

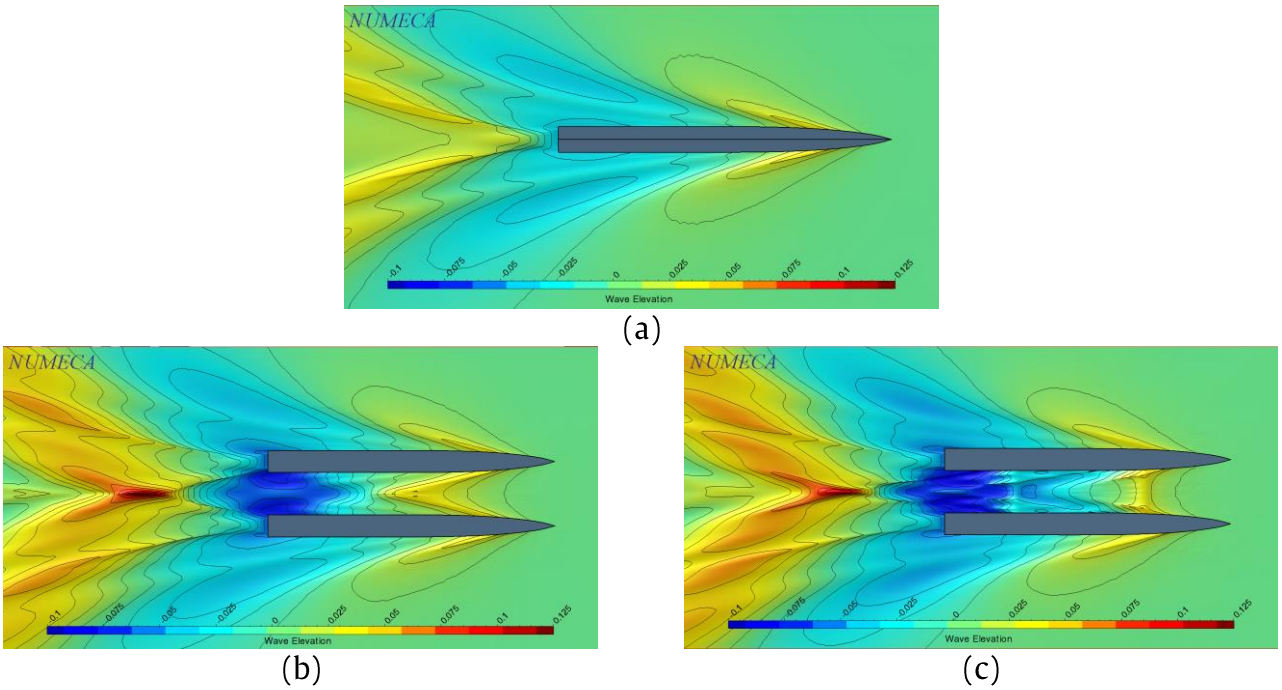

Figure 8. Wave elevation for the monohull (a), catamaran (b) and hysucat (c) at a speed of Fr 0.55

The statistics presented earlier indicate that although hydrofoils effectively reduce friction and wave resistance, they also lead to an increase in drag. At greater speeds, wave-making resistance becomes a significant factor in total resistance, consistent with prior study findings [35], [36], [37]. The research found that hydrofoil-supported catamarans had a distinct resistance profile compared to typical catamarans. The hydrofoil design provides for a drop in wetted surface area (WSA) as the ship accelerates, lowering overall resistance at certain speeds. However, this advantage is negated by the higher drag coefficient at all speeds caused by the hydrofoils' greater surface area and produced drag. Our investigation of the interference effects between hydrofoils and hulls demonstrates the complexities of hydrofoil-supported catamaran design. The interaction of hydrofoil-induced flow disturbances with the hull's boundary layer may cause more significant drag, particularly in catamarans with shorter hull separations. This indicates the necessity for rigorous design optimization to prevent these detrimental impacts. Furthermore, the analysis of wave fields created by these boats demonstrates that hydrofoil-supported catamarans exhibit unusual hydrodynamic behavior when compared to monohulls and standard catamarans. These results highlight the significance of evaluating the complete wave environment around the vessel as it determines total hydrodynamic performance.

4. Conclusion

This research presents critical insights into the hydrodynamics of hydrofoil-supported catamaran ships through comprehensive Computational Fluid Dynamics (CFD) simulations. Key findings include the observation that the total drag coefficient generally increases with speed, adhering to theoretical predictions that link resistance to the square of speed. Notably, at specific speeds, hydrofoil-supported catamarans (hysucats) demonstrate reduced total resistance compared to conventional catamarans, attributed to the hydrofoil's ability to lift part of the vessel above the water, lessening frictional and wave resistance. However, this lift generation inherently creates additional drag, particularly at high speeds, due to induced drag from the hydrofoil. The study also highlights the complex interplay between drag and lift forces from hydrofoils, which vary with speed and operational conditions. Notably, the interference between hydrofoils and hulls can lead to increased drag and reduced efficiency. Despite these challenges, strategic design optimizations show potential for minimizing adverse effects and enhancing overall efficiency. Future research should delve deeper into optimizing hydrofoil designs and configurations to strike a balance between drag and lift, ultimately improving the performance and efficiency of hydrofoil-supported catamarans in marine transportation.

Acknowledgments

The authors express gratitude to the Hydrodynamics Laboratory and Ship Design and Digitalization Laboratory Universitas Diponegoro for their assistance.

References

[1] A. Firdhaus and I. K. Suastika, "Experimental and Numerical Study of Effects of the Application of Hydrofoil on Catamaran Ship Resistance," in *The International Conference on Marine Technology (SENTA)*, Scitepress, 2022, pp. 104–110. doi: 10.5220/0010854400003261.

[2] K. Suastika, G. E. Nadapdap, M. H. N. Aliffrananda, Y. A. Hermawan, I. K. A. P. Utama, and W. D. Aryawan, "Resistance Analysis of a Hydrofoil Supported Watercraft (Hysuwac): A Case Study," *CFD Letters*, vol. 14, no. 1, pp. 87–98, 2022, doi: 10.37934/cfdl.14.1.8798.

[3] J.-B. R. G. Souppez, "Hydrofoil Configurations For Sailing Superyachts: Hydrodynamics, Stability And Performance," Design & Construction of Super and Mega Yachts 2019, 2019, doi: 10.3940/rina.smy.2019.05.
[4] J. R. Meyer, "Hybrid Hydrofoil Technology Applications," *Naval Engineers Journal*, vol. 106, no. 1, pp. 123–136, 1994, doi: 10.1111/j.1559-3584.1994.tb02803.x.
[5] JR. , J. Meyer and J. King, "The hydrofoil small waterplane area ship /HYSWAS/," in Advanced Marine Vehicles Conference, Reston, Virigina: American Institute of Aeronautics and Astronautics, Sep. 1976. doi: 10.2514/6.1976-875.
[6] K. G. W. Hoppe, "Recent Applications of Hydrofoil-Supported- Catamarans," Fast Ferry International, pp. 1–20, 2001.
[7] K. G. W. Hoppe, "Optimisation of Hydrofoil-Supported-Planing Catamarans," in Third International Conference on Fast Sea Transportation, 1995, pp. 25–27.
[8] D. E. Calkins, "HYCAT: Hybrid hydrofoil catamaran concept," *Ocean Engineering*, vol. 11, no. 1, pp. 1–21, 1984, doi: 10.1016/0029-8018(84)90021-0.
[9] H. Miyata, "Development of a New-Type Hydrofoil Catamaran," *Journal of Ship Research*, vol. 33, no. 02, pp. 135–144, 1989, doi: 10.5957/jsr.1989.33.2.135.
[10] S. Zaghi, R. Broglia, and A. Di Mascio, "Experimental and numerical investigations on fast catamarans interference effects," *Journal of Hydrodynamics*, vol. 22, no. 5 SUPPL. 1, pp. 528–533, 2010, doi: 10.1016/S1001-6058(09)60250-X.
[11] R. Broglia, S. Zaghi, and A. Di Mascio, "Numerical simulation of interference effects for a high-speed catamaran," Journal of Marine Science and Technology, vol. 16, no. 3, pp. 254–269, 2011, doi: 10.1007/s00773-011-0132-3.
[12] A. Doğrul, E. Kahramanoğlu, and F. Çakıcı, "Numerical prediction of interference factor in motions and added resistance for Delft catamaran 372," *Ocean Engineering*, vol. 223, p. 108687, Mar. 2021, doi: 10.1016/j.oceaneng.2021.108687.
[13] A. P. Veer, van 't, and F. R. Siregar, "The interaction effects on a catamaran travelling with forward speed in waves," 1995. [Online]. Available: https://api.semanticscholar.org/CorpusID:107831418
[14] P. Zhou, L. Liu, L. Guo, Q. Wang, and X. Wang, "Numerical Study on the Effect of Stern Flap for Hydrodynamic Performance of Catamaran," in Volume 2: CFD and FSI, American Society of Mechanical Engineers, 2019. doi: 10.1115/OMAE2019-96819.
[15] X. Wang, L. Liu, Z. Zhang, and D. Feng, "Numerical study of the stern flap effect on catamaran' seakeeping characteristic in regular head waves," *Ocean Engineering*, vol. 206, p. 107172, 2020, doi: 10.1016/j.oceaneng.2020.107172.
[16] N. Kumari and A. Chakraborty, "A Numerical Study of Flow Around Different Hydrofoil Systems In Presence of the Free Surface," in ASME 2021 Gas Turbine India Conference, American Society of Mechanical Engineers, 2021. doi: 10.1115/GTINDIA2021-75821.
[17] T. Castiglione, W. He, F. Stern, and S. Bova, "URANS simulations of catamaran interference in shallow water," *Journal of Marine Science and Technology*, vol. 19, no. 1, pp. 33–51, Mar. 2014, doi: 10.1007/s00773-013-0230-5.
[18] W. He, T. Castiglione, M. Kandasamy, and F. Stern, "Numerical analysis of the interference effects on resistance, sinkage and trim of a fast catamaran," *Journal of Marine Science and Technology*, vol. 20, no. 2, pp. 292–308, 2015, doi: 10.1007/s00773-014-0283-0.
[19] B. Bouscasse, R. Broglia, and F. Stern, "Experimental investigation of a fast catamaran in head waves," *Ocean Engineering*, vol. 72, pp. 318–330, 2013, doi: 10.1016/j.oceaneng.2013.07.012.
[20] R. Broglia, S. Zaghi, and F. Stern, "Calm Water and Seakeeping Investigation for a Fast Catamaran Coupling Potential Wave Models And Two-phase CFD Solvers with the SWENSE Methodology View project ONR-NICOP View project," 2011. [Online]. Available: https://www.researchgate.net/publication/266224698
[21] A. Firdhaus, Kiryanto, M. L. Hakim, G. Rindo, and M. Iqbal, "Ship Performances CFD Analysis of Hydrofoil-Supported High-Speed Catamaran Hull Form," *Journal of Advanced Research in Fluid Mechanics and Thermal Sciences*, vol. 113, no. 1, pp. 108–121, 2024, doi: 10.37934/arfmts.113.1.108121.
[22] R. van't Veer, "Experimental results of motions, hydrodynamic coefficients and wave loads on the 372 catamaran model," Wageningen, 1998.
[23] A. E. Ockfen and K. I. Matveev, "Aerodynamic characteristics of NACA 4412 airfoil section with flap in extreme ground effect," *International Journal of Naval Architecture and Ocean Engineering*, vol. 1, no. 1, pp. 1–12, 2009, doi: 10.2478/ijnaoe-2013-0001.
[24] A. Frère, K. Hillewaert, P. Chatelain, and G. Winckelmans, "High Reynolds Number Airfoil: From Wall-Resolved to Wall-Modeled LES," *Flow, Turbulence and Combustion*, vol. 101, no. 2, pp. 457–476, Sep. 2018, doi: 10.1007/s10494-018-9972-9.
[25] Abbot, H. Ira, and A. E. Von Doenhoff, Theory of Wing Sections (Including a Summary of Airfoil Data), New York, United States of America: Dover Publication, 1959.
[26] M. Effendy and Muchlisin, "Studi Eksperimental dan Simulasi Numerik Karakteristik Aerodinamika Airfoil NACA 4412," *ROTASI*, vol. 21, no. 3, pp. 147–124, 2019.
[27] M. N. Haque, M. Ali, and I. Ara, "Experimental Investigation on the Performance of NACA 4412 Aerofoil with Curved Leading Edge Planform," *Procedia Engineering*, vol. 105, pp. 232–240, 2015, doi: https://doi.org/10.1016/j.proeng.2015.05.099.
[28] H. K. Versteeg and W. Malalasekera, "Turbulence and its modeling," in An Introduction to Computational Fluid Dynamics, vol. 6, no. 4, 2007. doi: 10.1109/mcc.1998.736434.
[29] G. Jensen and H. Siding, "Rankine methods for the solution of the steady wave resistance problem," in *Proceedings 16th Symposium on Naval Hydrodynamics*, 1986, pp. 572–582.
[30] T. Li and J. Matusiak, "Simulation of modern surface ships with a wetted transom in a viscous flow," Proceedings of the *International Offshore and Polar Engineering Conference*, vol. 4, pp. 570–576, 2001.
[31] F. Menter, "Zonal Two Equation k-w Turbulence Models For Aerodynamic Flows," in 23rd Fluid Dynamics, Plasmadynamics, and Lasers Conference, in *Fluid Dynamics and Co-located Conferences*. , American Institute of Aeronautics and Astronautics, 1993. doi: doi:10.2514/6.1993-2906.

[32] F. R. Menter, "Two-equation eddy-viscosity turbulence models for engineering applications," *AIAA Journal*, vol. 32, no. 8, pp. 1598–1605, 1994, doi: 10.2514/3.12149.
[33] J. E. Bardina, P. G. Huang, and T. J. Coakley, "Turbulence modeling validation," *28th Fluid Dynamics Conference*, 2014, 1997, doi: 10.2514/6.1997-2121.
[34] R. Broglia, B. Jacob, S. Zaghi, F. Stern, and A. Olivieri, "Experimental investigation of interference effects for high-speed catamarans," *Ocean Engineering*, vol. 76, pp. 75–85, 2014, doi: 10.1016/j.oceaneng.2013.12.003.
[35] K. L. Wadlin, C. L. Shuford, and J. R. Mcgehee, "A Theoretical and Experimental Investigation of the Lift and Drag Characteristics of Hydrofoils at Subcritical and Supercritical Speeds," 1955. [Online]. Available: https://api.semanticscholar.org/CorpusID:121458541
[36] I. N. Ismail, P. Manik, and M. Indiaryanto, "Effect of the Addition of Hydrofoil on Lift Force and Resistance in 60 M High-Speed Vessel," *Kapal: Jurnal Ilmu Pengetahuan dan Teknologi Kelautan*, vol. 17, no. 3, pp. 95–106, 2020, doi: 10.14710/kapal.v17i3.28772.
[37] M. Haase, J. Binns, G. Thomas, N. Bose, G. Davidson, and S. Friezer, "On the macro hydrodynamic design of highly efficient medium- speed catamarans with minimum resistance," *International Journal of Maritime Engineering*, vol. 154, no. A3, 2021, doi: 10.5750/ijme.v154iA3.882.